


Cite this: *RSC Adv.*, 2023, **13**, 27792

Received 3rd August 2023  
Accepted 12th September 2023

DOI: 10.1039/d3ra05251f

rsc.li/rsc-advances

# Effect of modulation by adsorption and doping on the quantum capacitance of borophene

Guangmin Yang,<sup>a</sup> Xinlin Yang,<sup>a</sup> Zhuo Li,<sup>a</sup> Haihua Huang<sup>ID</sup><sup>b</sup> and Jianyan Lin<sup>ID</sup><sup>\*a</sup>

Electric double-layer supercapacitors (EDLCs) have attracted much attention in the energy storage field due to their advantages such as high output power, long service life, safety and high efficiency. However, their low energy density limits their application. Aiming at the problem of the low energy density of EDLCs, improving quantum capacitance ( $C_Q$ ) of electrode materials is an effective strategy. In this paper, we systematically studied the effects of vacancy, doping, and metal atom adsorption on the  $C_Q$  of borophene using first-principles calculations. The results show that S and N doping greatly enhance the charge accumulation of borophene at positive and negative potential, respectively. The maximum  $C_Q$  values of S-doped and N-doped borophene are  $157.3 \mu\text{F cm}^{-2}$  (0.38 V) and  $187.8 \mu\text{F cm}^{-2}$  (−0.24 V), respectively. Both of them can serve as ideal candidates for the positive (S-doped one) and negative (N-doped one) electrodes of EDLCs. Besides, metal Al atom-adsorbed borophene can also effectively enhance the  $C_Q$ , with a maximum value of  $109.1 \mu\text{F cm}^{-2}$ .

## 1. Introduction

With the increasingly serious environmental pollution and the rapid depletion of non-renewable energy, it is urgent to develop sustainable and clean energy sources.<sup>1</sup> However, the production of renewable energy (such as wind and solar energy) is discontinuous due to regional and temporal factors.<sup>2</sup> Therefore, the development of reliable, higher energy density and low-cost energy conversion and storage devices is rather important.<sup>3</sup> Among various energy storage devices, electric double-layer supercapacitors (EDLCs) have attracted much attention due to their high-power density and long cycle life. However, EDLCs usually exhibit lower energy densities.<sup>4</sup> Studies have shown that the electrode material of EDLCs is one of the most important factors limiting the energy density.<sup>5,6</sup>

Two-dimensional (2D) materials have promising application prospects as electrode materials due to their unique physical and chemical properties, including high specific surface area and good conductivity.<sup>7–11</sup> For 2D electrode materials, the total interfacial capacitance ( $C_T$ ) can be expressed as  $1/C_T = 1/C_Q + 1/C_D$ , where  $C_Q$  is the quantum capacitance, and  $C_D$  is the electric double layer capacitance.<sup>12–14</sup> The  $C_Q$  limits the total interface capacitance as much as the electric double layer capacitance. Therefore, it is necessary to improve the  $C_Q$  of 2D electrode materials. In recent years, researchers have modulated the  $C_Q$  of two-dimensional materials such as graphene, silicene and

germanene by means of defects and doping,<sup>15–17</sup> which makes a high density of electron states at the Fermi level.

Boron is the adjacent element of carbon. It has the same short covalent radius and the flexibility to adopt  $sp^2$  hybridization as carbon.<sup>18</sup> There are three valence electrons in the outer layer of boron, which could form a typical 2D configuration of borophene. *Ab initio* calculations were used by Boustania and Quandt to predict a variety of stable borophenes and boron nanotubes, which opened the curtain to the study of 2D boron sheets.<sup>19,20</sup> Different from graphene, intrinsic borophene is metallic and has electron density of states at the Fermi level.<sup>21</sup> Theoretical studies have shown that borophene may have a variety of allotropes. The common structures of borophene allotropes are triangular, hexagonal and triangular-hexagonal mixed structures.<sup>22–24</sup> Borophene can be made by various methods, such as chemical vapor decomposition on a metal substrate, molecular beam epitaxy, and liquid exfoliation, to produce 2D flat boron.<sup>25–29</sup> In 2015, Mannix *et al.*<sup>30</sup> successfully prepared wrinkled triangular borophene (2-*Pmmn*) on Ag (111) surface by experiments. In the same year, Tai *et al.*<sup>31</sup> prepared  $\gamma$ -B<sub>28</sub> with direct band gap on copper foils surface by chemical vapor deposition. In particular, Hou *et al.*<sup>32</sup> demonstrate that hydrogenated borophenes in large quantities can be prepared without any metal substrates by a stepwise *in situ* thermal decomposition of sodium borohydride under hydrogen as the carrier gas. And Liu *et al.*<sup>33</sup> confirmed through a CO-functionalized scanning tunneling microscopy that borophene is a chemically discrete two-dimensional material as opposed to a surface reconstruction or alloy with the underlying Ag(111) growth substrate. In addition, the single crystal boron nanoplate prepared by Zhai *et al.*<sup>34</sup> is a p-type semiconductor with

<sup>a</sup>College of Physics, Changchun Normal University, Changchun 130032, China. E-mail: linjy994@nenu.edu.cn

<sup>b</sup>School of Materials Science and Engineering, Liaocheng University, Liaocheng 252059, China



a carrier modulus of  $1.26 \times 10^{-1} \text{ cm}^2 \text{ V}^{-1} \text{ s}^{-1}$ , which has excellent electrical conductivity. The latest results that a 2D borophene supercapacitor prepared by Abdi *et al.*<sup>35</sup> reached a high specific capacitance of  $350 \text{ } \mu\text{F g}^{-1}$ , which clarified the application prospect of borophene-based supercapacitors.

In recent years, many studies have suggested that vacancy defects, atom doping, and functional group adsorption caused by chemical treatment during growth can effectively enhance the  $C_Q$  of the electrode materials. For instance, Zhou *et al.*<sup>36</sup> introduced vacancy defects into graphene, increasing the maximum  $C_Q$  from  $21.34 \text{ } \mu\text{F cm}^{-2}$  to  $120.72 \text{ } \mu\text{F cm}^{-2}$ . In our previous studies, introducing dopants into silicene with monovacancy defects also improved the  $C_Q$ .<sup>16</sup> The latest theoretical research shows that the  $C_Q$  of monolayer  $\delta$ -6 borophene is  $203.09 \text{ } \mu\text{F cm}^{-2}$ .<sup>37</sup> However, there is no detailed report on the effects of defects and doping on the  $C_Q$  of borophene.

In this work, we perform the first-principles method to investigate the effects of vacancy defects, metal atom adsorption (Ag, Au, Cu, Ti, Al) and doping (C, N, O, P, S) on the electronic structure and  $C_Q$  of 2-*Pmmn* borophene. By analyzing its electronic structure and fitting the changes of  $C_Q$  and surface storage charge with potential difference, its energy storage properties were explored. In addition, the co-doping of S (N) and Al and the adsorption of Al atoms on vacancy defects were studied. The results show that borophene has the best adsorption effect on Al, and the maximum  $C_Q$  is  $103.4 \text{ } \mu\text{F cm}^{-2}$ . S doping significantly improves the  $C_Q$  of borophene, and the maximum value reaches  $120.2 \text{ } \mu\text{F cm}^{-2}$ . When the concentration of S is increased to 4.17%, the  $C_Q$  is further increased to  $157.3 \text{ } \mu\text{F cm}^{-2}$ . Therefore, doping and adsorption can be used as an effective way to improve the energy storage performance of borophene-based supercapacitors.

## 2. Computational methods

In this work, we use the VASP package to perform first-principles calculations.<sup>38–40</sup> Projected augmented wave (PAW) method was used to optimize the geometric structure of the modulated borophene.<sup>41</sup> The exchange correlation energy of the interaction between electrons is expressed by the Perdew–Burke–Ernzerhoff (PBE) functional with the generalized gradient approximation (GGA).<sup>42,43</sup> In order to avoid the interaction between the layers, 20 Å vacuum layers were added. The *K*-point sampling in the Brillouin zone used the Monkhorst–Pack method. The energy convergence criterion of atomic relaxation was  $10^{-6} \text{ eV}$ , and the cutoff energy was set to 450 eV. The spin polarization was considered in our calculations. The van der Waals (vdW) interaction is considered with dispersion correction *via* the vdW-DF method.

The optimized lattice constants of 2-*Pmmn* borophene are  $a = 1.617 \text{ Å}$  and  $b = 2.867 \text{ Å}$ , which are consistent with the previously reported theoretical and experimental results.<sup>37,44–46</sup> Based on the original cell ( $1 \times 1$ ), a  $4 \times 4$  supercell is constructed. The adsorption energy of metal atoms adsorbed on intrinsic borophene is calculated by the following formula:

$$\Delta E_{\text{ad}}(x) = E_{\text{Bor-M}}(x) - E_{\text{Bor}} - \mu_{\text{M}} \quad (1)$$

$E_{\text{Bor}}$  and  $E_{\text{Bor-M}}$  are the total energy of intrinsic borophene and adsorbed by metal atoms, respectively, and  $\mu_{\text{M}}$  is the chemical potential of a single adsorbing atom (Ag, Au, Cu, Ti, Al).

The doping concentration is controlled by changing the size of the supercell. Formation energy was calculated to determine the stability of the defect structures. The formation energies of borophene with monovacancy, divacancy and dopants of C, N, O, P, S atoms are:

$$\Delta E_{\text{f}} = E_{\text{Bor-SV}} - (n - 1)\mu_{\text{B}} \quad (2)$$

$$\Delta E_{\text{f}} = E_{\text{Bor-DV}} - (n - 2)\mu_{\text{B}} \quad (3)$$

$$\Delta E_{\text{f}} = E_{\text{Bor-X}} - (n - 1)\mu_{\text{B}} - \mu_{\text{X}} \quad (4)$$

where  $E_{\text{Bor-SV}}$  and  $E_{\text{Bor-DV}}$  represent the total energy of borophene with monovacancy and divacancy,  $n$  is the number of B atoms in the original borophene,  $\mu_{\text{B}}$  is the energy of a single B atom, and  $\mu_{\text{X}}$  represents the energy of one doping atom (C, N, O, P, S).

The  $C_Q$  can be expressed as  $C_Q = d\sigma/d\Phi$ , where  $d\sigma$  and  $d\Phi$  represent the surface charge density and local potential, respectively.<sup>47,48</sup> According to the formula  $\mu = e\Phi$ , the electrochemical potential  $\mu_{\text{F}}$  can move rigidly through the local potential  $\Phi$ . On the electrode, the excess charge density can be expressed as:<sup>49</sup>

$$\Delta Q = -e \int_{-\infty}^{+\infty} D(E)[f(E) - f(E - e\Phi)]dE \quad (5)$$

$D(E)$  represent the electron density of states,  $e$  is the basic charge ( $e = 1.6 \times 10^{-19} \text{ C}$ ), and  $f(E)$  is the Fermi–Dirac distribution function.  $E$  is the relative energy of the Fermi level.<sup>16,49</sup> From this, the expression of  $C_Q$  is:

$$C_Q = e^2 \int_{-\infty}^{+\infty} D(E)F_{\text{T}}(E - e\Phi)dE \quad (6)$$

where  $F_{\text{T}}(E)$  is a thermal broadening function, denoted by:

$$F_{\text{T}}(E) = (4k_{\text{B}}T)^{-1} \text{sech}^2(E/2k_{\text{B}}T) \quad (7)$$

$k_{\text{B}}$  is the Boltzmann constant, and  $T$  is set to room temperature (300 K).

## 3. Results and discussion

### 3.1 The vacancy defects and adsorption of borophene

The structure of 2-*Pmmn* borophene shows a curved hexagonal structure (Fig. 1a), unlike silicene, its six-membered ring center is occupied by a boron atom. Each B atom in borophene is bonded to six adjacent atoms, the B1–B2 bond length on the same plane is  $1.617 \text{ Å}$ , which is slightly shorter than the B1–B3 ( $2.098 \text{ Å}$ ) on different planes. The two kinds of bond angles for each B atom are  $67.33^\circ$  and  $45.33^\circ$ , respectively.

In this section, we consider the monovacancy and two possible divacancy defects of 2-*Pmmn* borophene, as shown in Fig. 1b–d. The B1 and B2 atoms in the adjacent planes are deducted to form divacancy [110] (shown in Fig. 1c), and the absence of B1 and B3 atoms in the same plane is recorded as



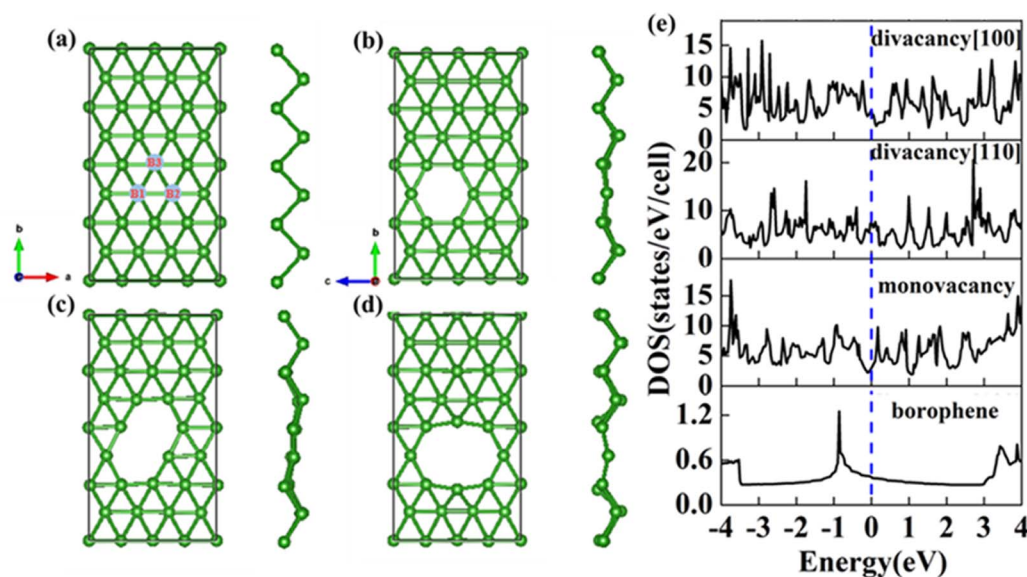


Fig. 1 Top view and side view of (a) pristine; (b) monovacancy; (c) divacancy [110]; (d) divacancy [100] borophene structures with a supercell of (4 × 4). (e) Electron density of states of the above four borophene structures.

divacancy [100] (shown in Fig. 1d). Fig. 1e shows the density of states of the four systems, since there is no band gap, the intrinsic borophene is metallic, which is consistent with the previous reports.<sup>19,30,50</sup> The density of states of monovacancy and divacancy [110] borophene near the Fermi level appear obvious decrease which is caused by the unoccupied state caused by the defect vacancy. We calculate the formation energy to describe the stability of different defects (Fig. 2a). In addition, four possible adsorption sites of borophene are marked in Fig. 2b. As we expected, defects are likely to cause instability of the 2D material structure. Contrary to what was thought, the divacancy seems to be more stable than the monovacancy for borophene, because of the formation energies of the two double-vacant structures are about six times lower than that of the monovacancy.

The  $C_Q$  with potential of intrinsic, monovacancy, divacancy [110] and [100] borophene is shown in Fig. 3a. The  $C_Q$  of intrinsic borophene shows an inclined straight line, which is stable with the increase of potential. For monovacant, divacant

[110] and [100] borophene, the local maximum values of  $C_Q$  are  $73.0 \mu\text{F cm}^{-2}$  (−0.17 V),  $83.8 \mu\text{F cm}^{-2}$  (0.24 V) and  $84.6 \mu\text{F cm}^{-2}$  (0.43 V), respectively. According to the relationship between surface charge density and potential calculated in Fig. 3b, the charge accumulation effect of intrinsic borophene is better than that of borophene structure after introducing vacancies. Different from other 2D materials, the influence of  $C_Q$  of borophene on vacancy defects is relatively stable.

In view of the high conductivity of transition metal atoms (Au, Ag, Cu, Ti, Al), we will discuss its adsorption effect on various adsorption sites of borophene. As schematic models shown in Fig. 2b, borophene has four adsorption sites, T1: above the top atom; T2: above the bottom atom; B1: above the top B–B bond; B2: above the bottom B–B bond. Similarly, we will judge the most stable situation of each atom in the above four positions by adsorption energy (Table 1). The negative adsorption energy advocates the feasibility of transition metal atoms adsorption. The adsorption energy of Ag, Cu, Al at T1 position is the lowest and the configuration is the most stable, but Au and

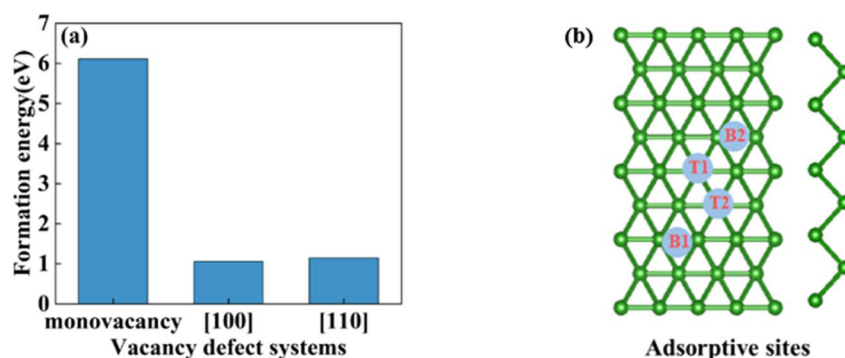


Fig. 2 (a) The formation energy of monovacancy, [110], [100] defect borophene; (b) four adsorption sites of borophene.



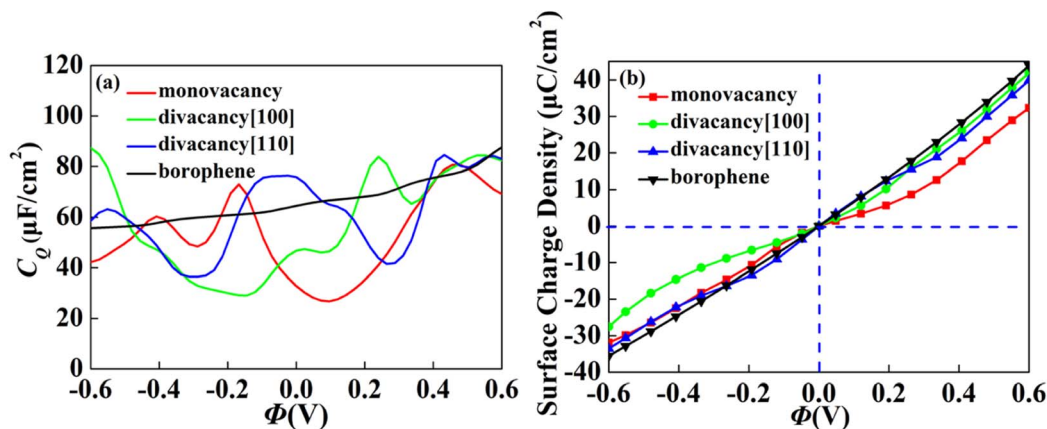


Fig. 3 The (a) quantum capacitance and (b) surface charge density changes of intrinsic, monovacancy, divacancy [110], divacancy [100] borophene with potential.

Table 1 The adsorption energy (eV) of Au, Ag, Cu, Ti and Al atoms adsorbed on borophene at T1, T2, B1 and B2 sites

$\Delta E_{\text{ad}}$	Au	Ag	Cu	Ti	Al
T1	-1.989	-1.663	-2.333	-4.184	-2.429
T2	-2.015	-1.815	-2.723	-4.827	-2.728
B1	-2.117	-1.704	-2.324	-3.236	-2.431
B2	-2.068	-1.778	-2.591	-5.173	-2.676

Ti are most stable at B1 and B2 positions, respectively. Based on the stable adsorption of the above atoms on intrinsic borophene, we further studied their effects on the electronic structure and  $C_Q$  (Fig. 4a and b). The adsorption is carried out on  $4 \times 4$  intrinsic borophene. Compared with pristine borophene, the adsorption of Au, Ag, Cu caused a decrease in the density of states near the Fermi level, resulting in a decrease in the  $C_Q$  at zero potential, and the overall trend was relatively the same, but the Au adsorption system had a relatively good effect

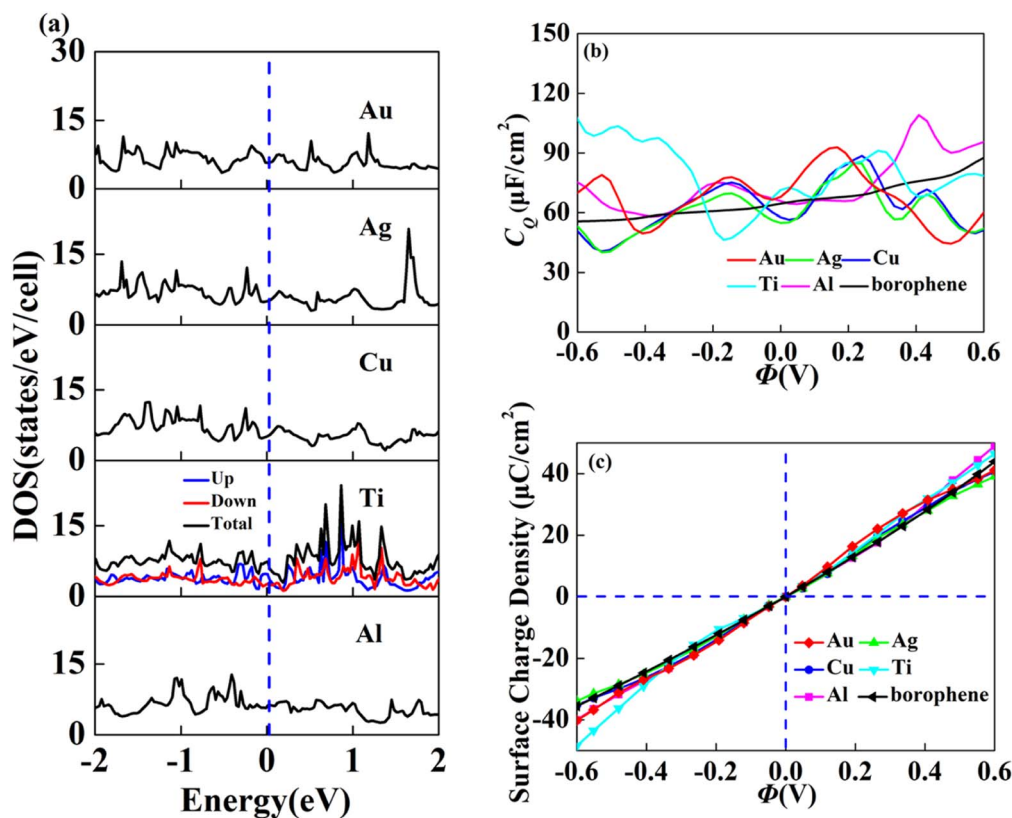


Fig. 4 The (a) electronic density of states, (b) quantum capacitance and (c) surface charge density of borophene adsorbing Au, Ag, Cu, Ti, Al.



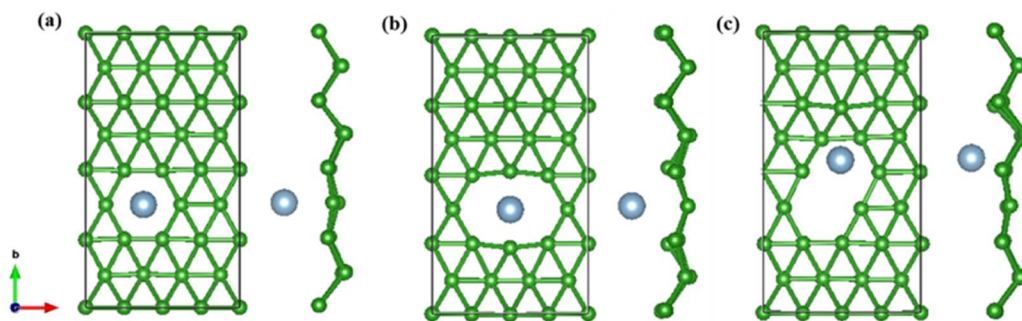


Fig. 5 The optimized structure of (a) monovacancy, (b) divacancy [100], (c) divacancy [110] borophene adsorbed Al in  $4 \times 4$  supercell.

on charge accumulation (Fig. 4c). The adsorption of Ti and Al atoms improves the  $C_Q$  of borophene, and the local maximum values are  $103.5 \mu\text{F cm}^{-2}$  ( $-0.48 \text{ V}$ ) and  $109.1 \mu\text{F cm}^{-2}$  ( $0.45 \text{ V}$ ), respectively. This is attributed to the local electronic state formed near the zero potential. At the same time, the charge stored from their surface can verify that Ti, Al doped borophene has the potential to be a symmetrical supercapacitor electrode.

On the whole, the effect of intrinsic borophene adsorbing Al is the best. Therefore, we consider adsorbing Al in borophene containing vacancy defects. The adsorption configuration on monovacancy, divacancy [100] and divacancy [110] is shown in Fig. 5a–c. The stable adsorption site is at top of monovacancy for monovacancy borophene (Fig. 5a), the center of vacancy for divacancy [100] (Fig. 5b), and the off-center of vacancy for divacancy [110] (Fig. 5c), respectively. In order to intuitively show the electronic properties, we draw the energy band structure diagram of three kinds of vacancy adsorption Al in Fig. 6a–c. The energy band of these three materials cross the Fermi level and exhibit metallic character. The  $C_Q$  and charge density of divacancy [100] borophene are enhanced under negative potential after adsorbing Al, the capacitance value is  $87.8 \mu\text{F cm}^{-2}$  ( $-0.096 \text{ V}$ ), while the  $C_Q$  of [110] borophene peaked at  $83.1 \mu\text{F cm}^{-2}$  at  $0.12 \text{ V}$  (Fig. 7a). Through surface charge storage (Fig. 7b), it is found that Al adsorbed [100] and [110] borophene are suitable for the negative and positive electrodes of supercapacitors, respectively.

### 3.2 The doping and co-doping of borophene

For 2D materials, the light element (such as N, P, S) doping is one of the common strategies usually used to regulate the electronic properties of materials. Combined with the

characteristics of B, we take C and O into account and consider the effect of doping on the  $C_Q$  of borophene. Fig. 8a–e depicted the quantum capacitance of C, N, O, P, S doped borophene. Firstly, we calculated the defect formation energy, as shown in Fig. 9a, and concluded that the formation energy of O doping is the lowest. For intrinsic borophene, when the local potential is zero, a lower  $C_Q$  appears, and the trend is symmetrical U-shaped. The local maximum values of the doped  $C_Q$  are  $83.8 \mu\text{F cm}^{-2}$  ( $0.05 \text{ V}$ ),  $90.3 \mu\text{F cm}^{-2}$  ( $-0.29 \text{ V}$ ),  $94.5 \mu\text{F cm}^{-2}$  ( $0.17 \text{ V}$ ),  $110.9 \mu\text{F cm}^{-2}$  ( $0.17 \text{ V}$ ) and  $120.2 \mu\text{F cm}^{-2}$  ( $0.05 \text{ V}$ ), respectively. Obviously, the introduction of non-metallic atoms improves the  $C_Q$  of intrinsic borophene. The improvement of  $C_Q$  is due to the downward shift of Fermi level and the formation of nearby localized states. Fig. 9b and c shows the change of surface charge density with potential. Under positive potential, the charge accumulation effect of S and N doping is obviously enhanced, in particular, the surface charge density of the S-doped system reaches  $60 \mu\text{C cm}^{-2}$  at  $0.6 \text{ V}$ , and the enhancement effect of N doping is the best under negative potential. It shows that S and N doped borophene have the potential to be used as positive and negative electrodes for supercapacitors, respectively. In order to further analyze the effect of doping on the electronic structure of borophene, we plotted the energy band diagram of the doped structure as shown in Fig. 10a–f. The band structure of intrinsic borophene again verifies its metallicity, but doped atoms not only produce deep localized states, but also make the electronic structure redistributing. The doping of P and S leads to higher local states near the Fermi level. The density of states shows a downward trend near the conduction band minima, indicating that the electrons occupying the lower part are delocalized. But in general, doping does

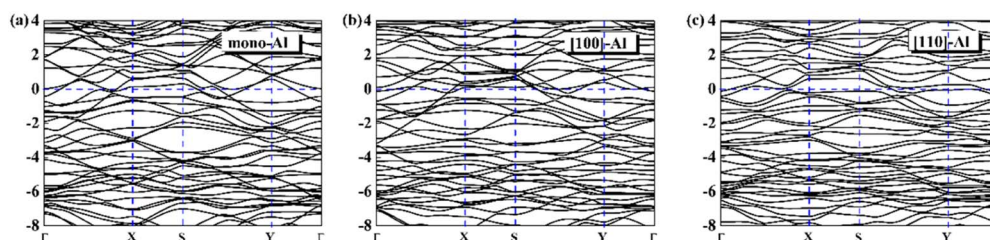


Fig. 6 The band structure diagram of (a) monovacancy, (b) divacancy [100], (c) divacancy [110] borophene adsorbed Al.



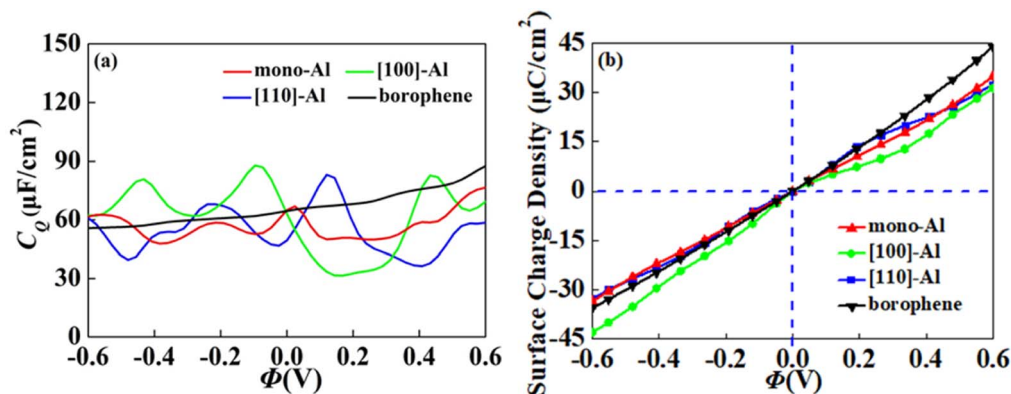


Fig. 7 The (a) quantum capacitance and (b) surface charge density of Al adsorbed on vacancy borophene.

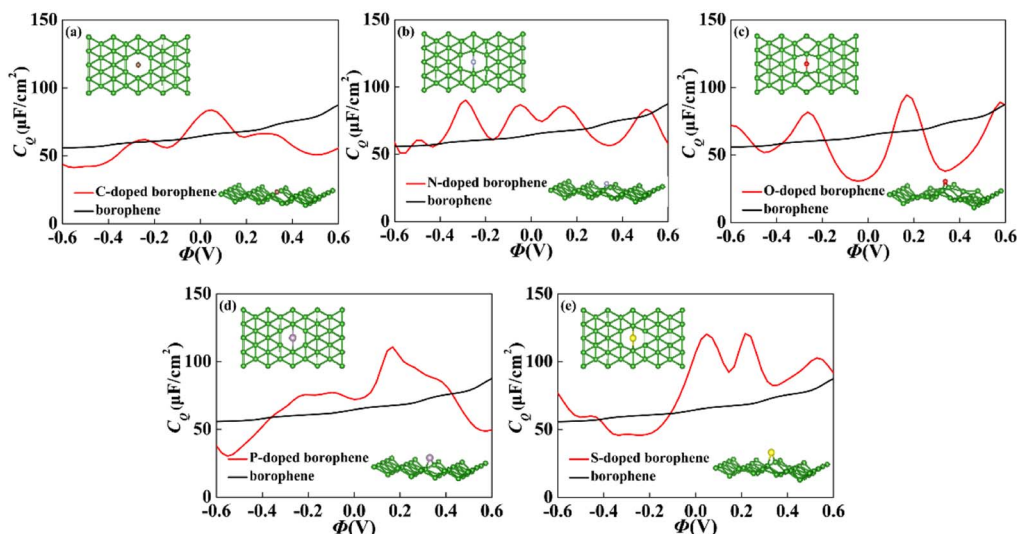


Fig. 8 The crystal structure and change of quantum capacitance of (a) C, (b) N, (c) O, (d) P, (e) S doped borophene with potential.

not change the metallic behavior of borophene. From Pauling's chemical bond theory, this is because boron is an electron-deficient substance, and the doped atoms do not affect the conjugated  $\pi$  bond in borophene, and the electronic structure of borophene will not change significantly.<sup>51</sup>

In order to further explore the concentration effect of doping on borophene  $C_Q$ , we construct the  $4 \times 4$ ,  $4 \times 3$  and  $3 \times 3$

supercell structures, corresponding concentration of 3.13%, 4.17% and 5.56%, respectively. When the S doping concentration is 4.17% and 5.56%, the  $C_Q$  values of  $157.3 \mu\text{F cm}^{-2}$  (0.38 V) and  $122.7 \mu\text{F cm}^{-2}$  (−0.31 V) are higher, which are twice the intrinsic  $C_Q$  at the same potential. The charge accumulation effect after S doping, as shown in Fig. 11b, is significantly enhanced at 4.17% positive potential. Under negative potential,

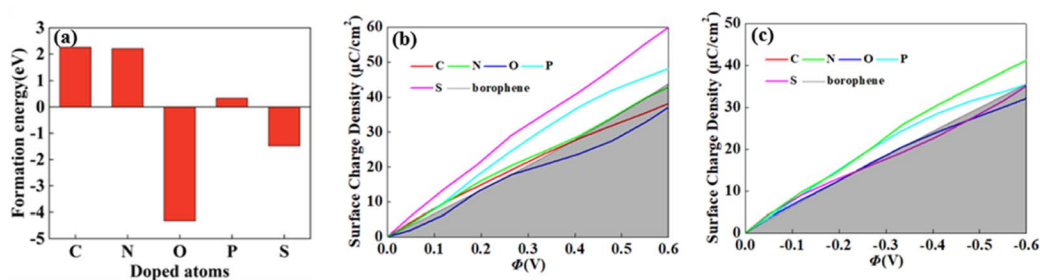


Fig. 9 The (a) formation energy and change of surface charge density with (b) positive, (c) negative potential of C, N, O, P, S doped borophene.

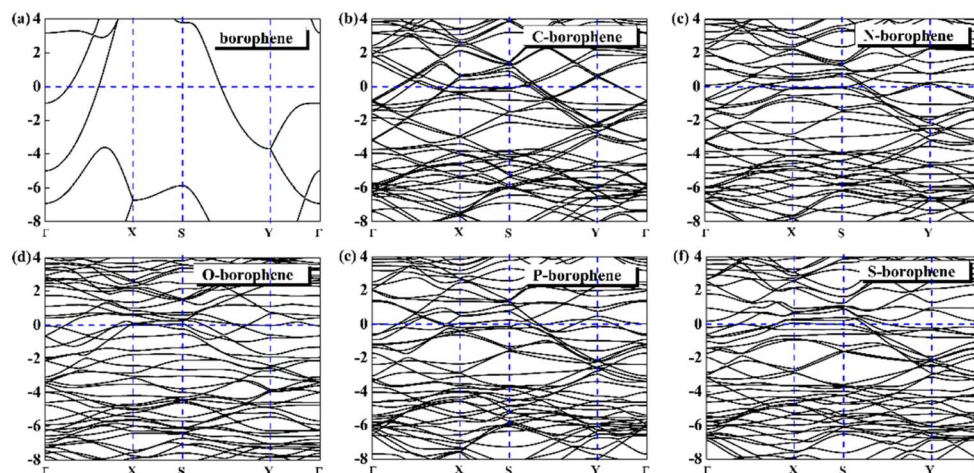


Fig. 10 The band structure diagram of (a) intrinsic borophene and doped (b) C, (c) N, (d) O, (e) P, (f) S atom.

5.56% S doping has the best enhancement effect. Therefore, borophene can be applied to the positive and negative electrodes of supercapacitors by controlling the N doping concentration. After N doping, the  $C_Q$  value gradually increases with the increase of concentration. When the doping concentration is 5.56%, the  $C_Q$  increases most obviously, reaching a maximum value of  $187.8 \mu\text{F cm}^{-2}$  ( $-0.24 \text{ V}$ ). The surface charge density in Fig. 11d also corresponds to it, indicating that borophene

with N doping concentration of 4.17% has more advantages in the negative electrode of supercapacitors.

Combined with the excellent energy storage effect of Al adsorbed borophene mentioned above, we combined it with S and N doped borophene with different concentrations. The synergistic effect both of aspects are considered. We selected the doping borophene structure ( $4 \times 3$  and  $3 \times 3$  borophene structure doped with S and N, respectively) with higher  $C_Q$  to

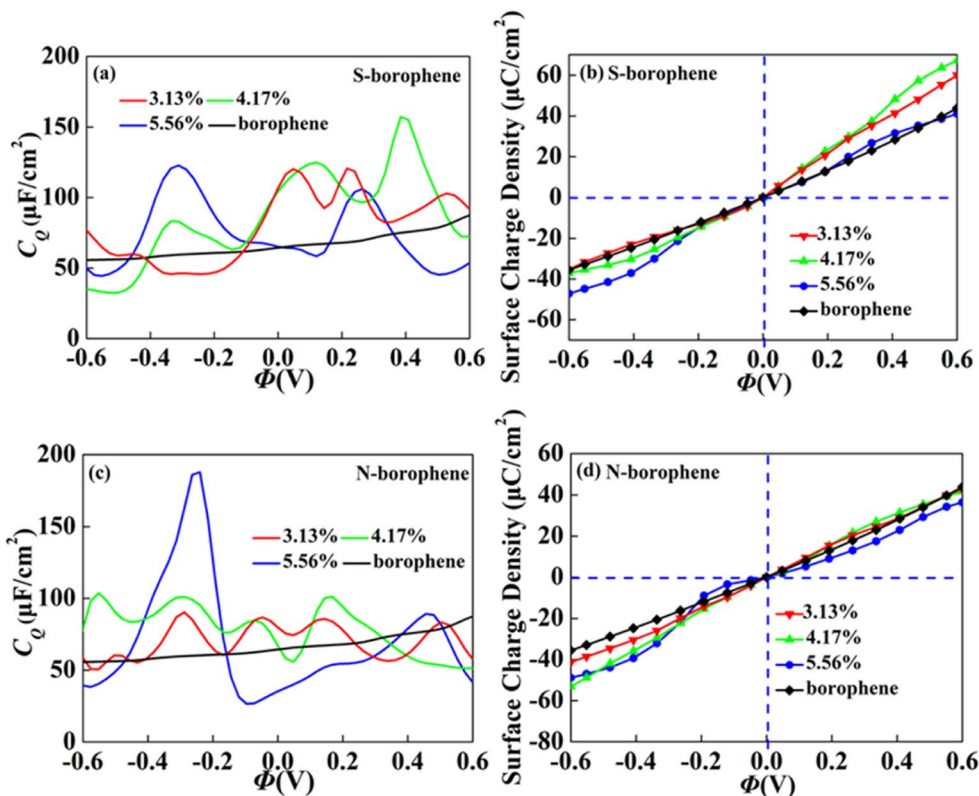


Fig. 11 The relationship between (a and c) quantum capacitance and (band d) surface charge density and potential of S, N doped borophene with different concentrations.





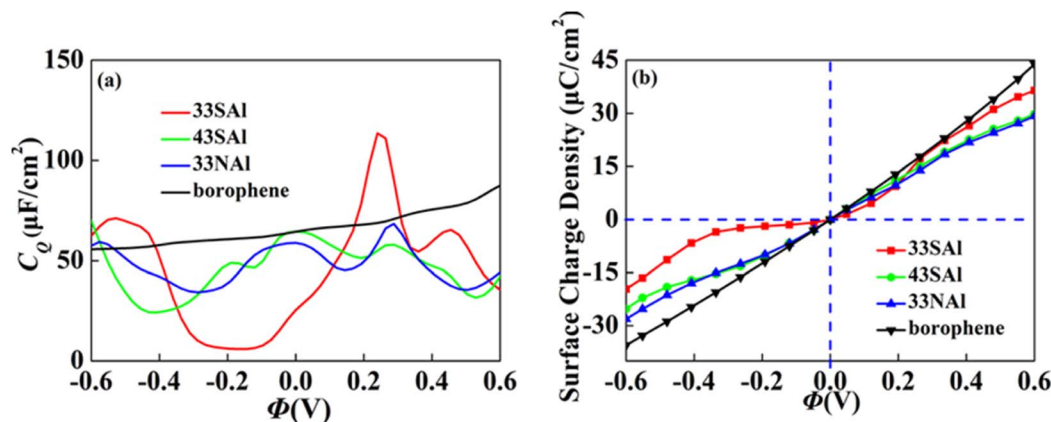


Fig. 12 The (a) quantum capacitance and (b) surface charge density of S, N doped borophene adsorbed Al.

adsorbed. The  $4 \times 3$  S doped borophene supercell with Al adsorption,  $4 \times 3$  S doped borophene supercell with Al adsorption, and  $4 \times 3$  N doped borophene supercell with Al adsorption are denoted 43SAI, 33SAI and 33NAI, respectively. After co-doping, the  $C_Q$  of 33SAI doped borophene reaches the maximum value of  $113.6 \mu\text{F cm}^{-2}$  ( $-0.24 \text{ V}$ ) at positive potential, but decreases sharply at negative potential, and the  $C_Q$  value is unstable, which may be caused by the local state of density of states (Fig. 12). Unfortunately, Al does not have a good positive effect on S and N-doped borophene, but the short-term improvement of 33SAI proves that co-doping is still a direction to be explored.

## 4. Conclusions

In summary, we systematically studied the effects of vacancy, adsorbed transition metal atoms (Au, Ag, Cu, Ti, Al) and doping (C, N, O, P, S) on the electronic structure and  $C_Q$  of borophene through first-principles calculations to improve the energy storage properties of borophene-based electrode materials. The results show that the vacancy defects have little effect on the  $C_Q$  of borophene electrode materials, but doping and adsorption can still effectively regulate the electronic structure of borophene, thereby improving its  $C_Q$ . In the system of metal atoms adsorbed borophene, the Al-adsorbed borophene exhibits excellent energy storage properties, and the  $C_Q$  reaches  $109.1 \mu\text{F cm}^{-2}$ . In the doped system, the maximum  $C_Q$  of S-doped borophene is  $120.2 \mu\text{F cm}^{-2}$ . Further increase the S doping concentration to 4.17%, the  $C_Q$  value is  $157.3 \mu\text{F cm}^{-2}$ . And by controlling the concentration of S-doped, borophene can be applied to the positive (4.17% one) and negative (5.56% one) electrodes of EDLCs respectively. The  $C_Q$  of N-doped borophene increases with the increase of concentration, and reaches the maximum value of  $87.8 \mu\text{F cm}^{-2}$  at the concentration of 5.56%, however, the surface charge density is the largest when the concentration is 4.17%. Nevertheless, N-doped borophene can still be regarded as an ideal anode material for supercapacitors.

## Conflicts of interest

The authors declare no competing financial interest.

## Acknowledgements

This work was supported by the Natural Science Foundation of Jilin Province (Grant No. YDZJ202201ZYT576).

## References

- 1 S. T and K. Tarafder, *Phys. B*, 2021, **604**, 412676.
- 2 R. M. Hu and J. X. Shang, *Appl. Surf. Sci.*, 2019, **496**, 143659.
- 3 C. Hou, G. Tai, Y. Liu, Z. Wu, X. Liang and X. Liu, *Nano Res. Energy*, 2023, **2**, e9120051.
- 4 C. Wang, Y. Zhou, L. Sun, Q. Zhao, X. Zhang, P. Wan and J. Qiu, *J. Phys. Chem. C*, 2013, **117**, 14912–14919.
- 5 L. L. Zhang and X. S. Zhao, *Chem. Soc. Rev.*, 2009, **38**, 2520–2531.
- 6 F. Béguin, V. Presser, A. Balducci and E. Frackowiak, *Adv. Mater.*, 2014, **26**, 2283.
- 7 B. Biel, X. Blase, F. Triozon and S. Roche, *Phys. Rev. Lett.*, 2009, **102**, 096803.
- 8 C. Liu, Z. Yu, D. Neff, A. Zhamu and B. Z. Jang, *Nano Lett.*, 2010, **10**, 4863–4868.
- 9 H. M. Jeong, J. W. Lee, W. H. Shin, Y. J. Choi, H. J. Shin, J. K. Kang and J. W. Choi, *Nano Lett.*, 2011, **11**, 2472–2477.
- 10 Y. Chen, X. Zhang, D. Zhang, P. Yu and Y. Ma, *Carbon*, 2011, **49**, 573–580.
- 11 J. Xia, F. Chen, J. Li and N. Tao, *Nat. Nanotechnol.*, 2009, **4**, 505–509.
- 12 A. J. Pak, E. Paek and G. S. Hwang, *Phys. Chem. Chem. Phys.*, 2013, **15**, 19741–19747.
- 13 G. M. Yang, H. Z. Zhang, X. F. Fan and W. T. Zheng, *J. Phys. Chem. C*, 2015, **119**, 6464–6470.
- 14 S. M. Mousavi-Khoshdeld and E. Targholi, *Carbon*, 2015, **89**, 148–160.
- 15 X. Si, Z. Li, S. Q. Wang, Q. Xu, J. Y. Lin and G. M. Yang, *Appl. Surf. Sci.*, 2022, **605**, 154673.
- 16 G. M. Yang, Q. Xu, X. F. Fan and W. T. Zheng, *J. Phys. Chem. C*, 2018, **122**, 1903–1912.
- 17 X. Si, W. She, Q. Xu, G. Yang, Z. Li, S. Wang and J. Luan, *Materials*, 2022, **15**, 103.
- 18 H.-J. Zhai, Y.-F. Zhao, W.-L. Li, Q. Chen, H. Bai, H.-S. Hu, Z. A. Piazza, W.-J. Tian, H.-G. Lu, Y.-B. Wu, Y.-W. Mu,





- G.-F. Wei, Z.-P. Liu, J. Li, S.-D. Li and L.-S. Wang, *Nat. Chem.*, 2014, **6**, 727–731.
- 19 I. Boustani, A. Quandt, E. R. Hernández and Á. Rubio, *J. Chem. Phys.*, 1999, **110**, 3176–3185.
- 20 I. Boustani, A. Quandt and Á. Rubio, *IEEE J. Solid-State Circuits*, 2000, **154**, 269–274.
- 21 H. Tang and S. Ismail-Beigi, *Phys. Rev. Lett.*, 2007, **99**, 115501.
- 22 B. Feng, J. Zhang, Q. Zhong, W. Li, S. Li, H. Li, P. Cheng, S. Meng, L. Chen and K. Wu, *Nat. Chem.*, 2016, **8**, 563–568.
- 23 J. He, D. F. Li, Y. Ying, C. B. Feng, J. J. He, C. Y. Zhong, H. B. Zhou, P. Zhou and G. Zhang, *npj Comput. Mater.*, 2019, **5**, 47.
- 24 C. Hou, G. Tai, Y. Liu, Z. Wu, Z. Wu and X. Liang, *J. Mater. Chem. A*, 2021, **9**, 13100–13108.
- 25 S.-Y. Xie, Y. Wang and X.-B. Li, *Adv. Mater.*, 2019, **31**, 1900392.
- 26 T. Z. Wen, A. Z. Xie, J. L. Li and Y. H. Yang, *Int. J. Hydrogen Energy*, 2020, **45**, 29059–29069.
- 27 C. Li, A. K. Tareen, K. Khan, J. Long, I. Hussain, M. F. Khan, M. Iqbal, Z. Xie, Y. Zhang, A. Mahmood, N. Mahmood, W. Ahmad and H. Zhang, *Prog. Solid State Chem.*, 2023, **70**, 100392.
- 28 Y. Jiao, F. Ma, J. Bell, A. Bilic and A. Du, *Angew Chem. Int. Ed.*, 2016, **55**, 10292–10295.
- 29 J. Joseph, V. S. Sivasankarapillai, S. Nikazar, M. S. Shanawaz, A. Rahdar, H. Lin and G. Z. Kyzas, *ChemSusChem*, 2020, **13**, 3754–3765.
- 30 A. J. Mannix, X. F. Zhou, B. Kiraly, J. D. Wood, D. Alducin, B. D. Myers, X. Liu, B. L. Fisher, U. Santiago, J. R. Guest, M. J. Yacaman, A. Ponce, A. R. Oganov, M. C. Hersam and N. P. Guisinger, *Science*, 2015, **350**, 1513–1516.
- 31 G. Tai, T. Hu, Y. Zhou, X. Wang, J. Kong, T. Zeng, Y. You and Q. Wang, *Angew. Chem., Int. Ed.*, 2015, **54**, 15473–15477.
- 32 C. Hou, G. Tai, J. Hao, L. Sheng, B. Liu and Z. Wu, *Angew. Chem., Int. Ed.*, 2020, **59**, 10819–10825.
- 33 X. Liu, L. Wang, S. Li, M. S. Rahn, B. I. Yakobson and M. C. Hersam, *Nat. Commun.*, 2019, **10**, 1642.
- 34 J. Xu, Y. Chang, L. Gan, Y. Ma and T. Zhai, *Adv. Sci.*, 2015, **2**, 1500023.
- 35 Y. Abdi, A. Mazaheri, S. Hajibaba, S. Darbari, S. J. Rezvani, A. D. Cicco, F. Paparoni, R. Rahighi, S. Gholipour, A. Rashidi, M. M. Byranvand and M. Saliba, *ACS Mater. Lett.*, 2022, **4**, 1929–1936.
- 36 Q. X. Zhou, W. W. Ju, Y. X. Liu, J. H. Li and Q. Zhang, *Appl. Surf. Sci.*, 2020, **510**, 145448.
- 37 H. Kolavada, S. Singh, I. Lukačević, P. N. Gajjar and S. K. Gupta, *Electrochim. Acta*, 2023, **439**, 141589.
- 38 G. Kresse and J. Furthmüller, *Comput. Mater. Sci.*, 1996, **6**, 15–50.
- 39 G. Kresse and J. Furthmüller, *Phys. Rev. B: Condens. Matter Mater. Phys.*, 1996, **54**, 11169–11186.
- 40 G. Kresse and J. Hafner, *Phys. Rev. B: Condens. Matter Mater. Phys.*, 1993, **47**, 558–561.
- 41 P. E. Blochl, *Phys. Rev. B: Condens. Matter Mater. Phys.*, 1994, **50**, 17953–17979.
- 42 P. Hohenberg and W. Kohn, *Phys. Rev.*, 1964, **136**, B864–B871.
- 43 J. P. Perdew, J. A. Chevary, S. H. Vosko, K. A. Jackson, M. R. Pederson, D. J. Singh and C. Fiolhais, *Phys. Rev. B: Condens. Matter Mater. Phys.*, 1992, **46**, 6671–6687.
- 44 B. Peng, H. Zhang, H. Z. Shao, Y. F. Xu, R. J. Zhang and H. Y. Zhua, *J. Mater. Chem. C*, 2016, **4**, 3592–3598.
- 45 H. X. Zhong, K. X. Huang, G. D. Yu and S. J. Yuan, *Phys. Rev. B*, 2018, **98**, 054104.
- 46 Q. X. Zhou, L. Wang, W. W. Ju, Y. L. Yong, S. L. Wu, S. T. Cai and P. C. Li, *Electrochim. Acta*, 2022, **433**, 141261.
- 47 E. Paek, A. J. Pak, K. E. Kweon and G. S. Hwang, *J. Phys. Chem. C*, 2013, **117**, 5610–5616.
- 48 X. Si, Q. Xu, J. Lin and G. Yang, *Appl. Surf. Sci.*, 2023, **618**, 156586.
- 49 D. L. John, L. C. Castro and D. L. Pulfrey, *J. Appl. Phys.*, 2004, **96**, 5180–5184.
- 50 P. Xiang, X. Chen, W. Zhang, J. Li, B. Xiao, L. Li and K. Deng, *Phys. Chem. Chem. Phys.*, 2017, **19**, 24945–24954.
- 51 L. C. Pauling, *Nature of the Chemical Bond*, Cornell University Press, Ithaca, NY, 1939.

